Supplementary information for

Full-Visible Multifunctional Aluminium Metasurfaces by In Situ Anisotropic Thermoplasmonic Laser Printing

Yinan Zhang[1], Liu Shi[1,2], Dejiao Hu[1], Shiren Chen[1], Shouyi Xie[3], Yudong Lu[1], Yaoyu Cao[1], Zhuqing Zhu[2], Long Jin[1], Bai-Ou Guan[1], Sven Rogge[3], and Xiangping Li[1*]

[1]Guangdong Provincial Key Laboratory of Optical Fiber Sensing and Communications, Institute of Photonics Technology, Jinan University, Guangzhou, China, 510632

[2]Department of Physics, Nanjing Normal University, Nanjing, China

[3]School of Physics, The University of New South Wales, Sydney 2052, Australia

**Corresponding author: xiangpingli@jnu.edu.cn;*

Supplementary discussion

Thermoplasmonic absorption. The metal-insulator-metal (MIM) configuration can support Fabry-Perot (FP) resonances and significantly enhance the absorption at the resonant wavelength. The electric field is mainly confined at the sharp curvatures of the nanostructures and absorbed pulse energy is dominantly dissipated in the top Al nanorods, which is responsible for Joule heating (Fig. S1). To calculate the temperature distribution, the absorbed energy was obtained by solving the full vector Maxwell equations using the Finite-difference time-domain (FDTD) method. The transient absorbed pulse energy responsible for subsequent thermoplasmonic

heating was then calculated by using the following equation [1]

$$Q(t) = \frac{\omega}{2}\varepsilon_0 \varepsilon''(\omega)|E(\omega,t)|^2 \quad \text{(S1)}$$

where ω is the angular frequency, ε'' is the imaginary part of the dielectric function, ε_0 is the permittivity of vacuum and $E(\omega,t)$ is the time-varying electric field.

Surface diffusion below the bulk melting temperature. The core of curvature-driven surface diffusion is to minimize the surface energy [2, 3], which has been recently adopted for modeling low-temperature stability of gold nanorods [4]. The outward atom migration speed of a point on the surface can be given as

$$\frac{dn}{dt} = -\nabla \cdot J_s \quad \text{(S2)}$$

$$J_s = -\frac{\Omega V_s}{kT} D_s \cdot \nabla\mu \quad \text{(S3)}$$

where Ω is the atomic volume, V_s is the number of diffusing surface atoms per unit area (normally $V_s = \Omega^{-2/3}$), k is the Boltzman's constant, T is the temperature, μ is the chemical potential and D_s is the surface self-diffusion coefficient which is assumed isotropic. Generally, it is temperature dependent following the Arrhenius behavior as

$$D_s(T) = D_0 exp^{(-E_a/kT)} \quad \text{(S4)}$$

where E_a is the activation energy and D_0 is a constant. Following the Herring's formula [2, 3], the chemical potential of an isotropic surface can be simplified as

$$\mu = \mu_0 + \gamma_s \Omega \mathrm{K} \quad \text{(S5)}$$

where μ_0 is the chemical potential of a flat surface, γ_s is the free energy and

$\mathrm{K} = \frac{1}{R_x} + \frac{1}{R_y}$ is the mean curvature of the surface. Finally, Eq. (S2) can be simplified as

$$\frac{dn}{dt} = \frac{\Omega^{4/3}\gamma_s D_s}{kT}\nabla^2 \mathrm{K} \tag{S6}$$

The Eq. (S6) clearly reveals the nature of the curvature-driven surface atom migration, which can be used to calculate the movement of the entire surface at fast temperature sweep given by the two-temperature model (TTM).

Two-temperature model. After the absorption of the 100 fs pulse, the thermoplasmonic heating effect first heats the conduction electrons. The subsequent energy exchange between electrons and atomic vibrations rises the lattice temperature of Al atoms. Concurrently, the lattice atoms cool down by phonon-phonon collisions between Al atoms and heat dissipation into the surrounding medium. This thermodynamic process can be described by the simplified TTM [1, 5-7]:

$$C_e\frac{\partial T_e}{\partial t} = -G_{el}(T_e - T_l) + Q(t)$$

$$C_l\frac{\partial T_l}{\partial t} = G_{el}(T_e - T_l) - (T_l - T_0)/\tau_s \tag{S7}$$

where T_e, T_l and T_0 are the electron temperature, lattice temperature and ambient temperature, respectively; C_e and C_l are the heat capacities (per unit volume) of the electron and lattice subsystems, respectively; G_{el} is the electron-lattice coupling coefficient; τ_s is the characteristic time of heat dissipation into ambient environment. In the temperature range of several thousands of Kelvin, $C_e = \gamma T_e$ is the electron heat capacity at different temperatures. The fast temperature sweep within the Al

nanostructures can be calculated using Eq. (S7). The parameters are $C_l = 2.42 \times 10^6 J/(m^3K)$ $G_{el} = 5.69 \times 10^{17} J/(m^3Ks)$, $\gamma = 134.5\, J/(m^3K^2)$, for Al[8]. Considering the thermal conductivity of the SiO_2 substrate, the characteristic decay time τ_s is set 700 ps obtained from simulation. The calculated results are shown in Supplementary Fig. S2.

Supplementary Figures

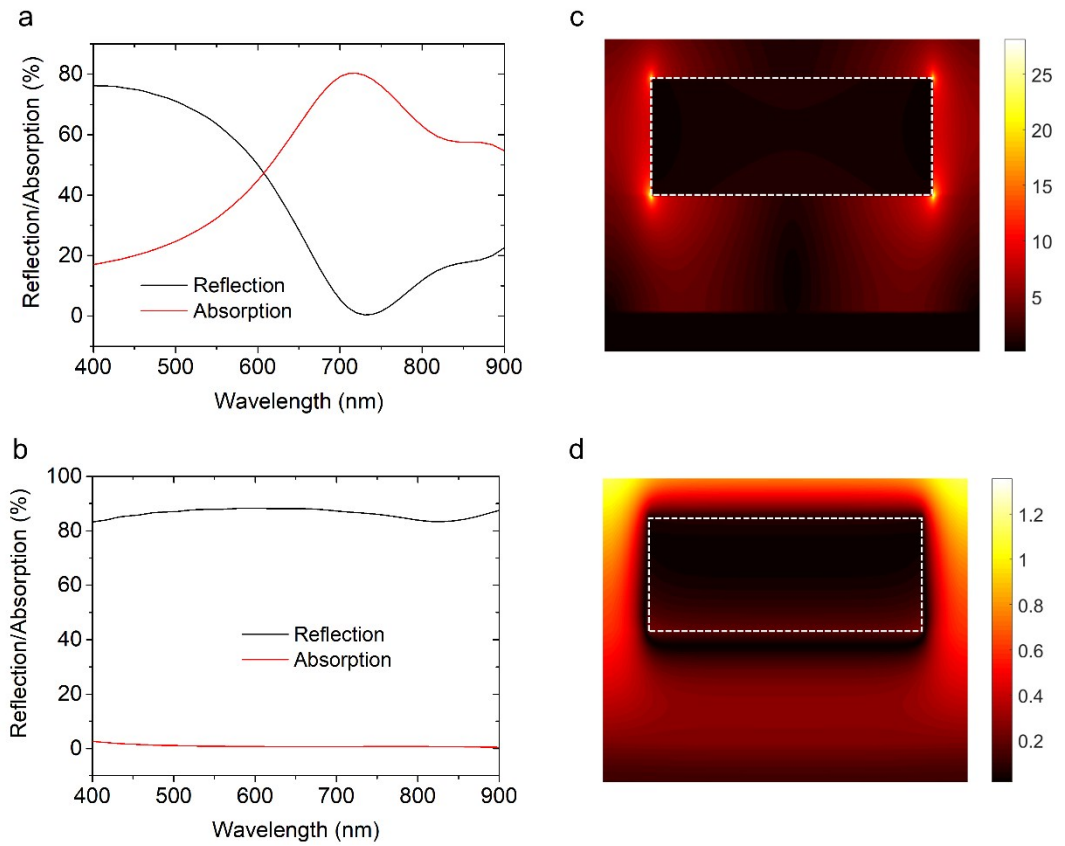

Supplementary Figure S1. Reflection and absorption spectra of the Al nanorod array under irradiance with polarization parallel (a) and perpendicular (b) to its longitudinal axis. The simulated electric field distribution at the wavelength of 730 nm under irradiance with polarization parallel (c) and perpendicular (d) to its longitudinal axis.

By switching the polarization of incidence, the absorption spectra exhibit a distinct contrast accompanied with an order of magnitude difference in confined electric field strength.

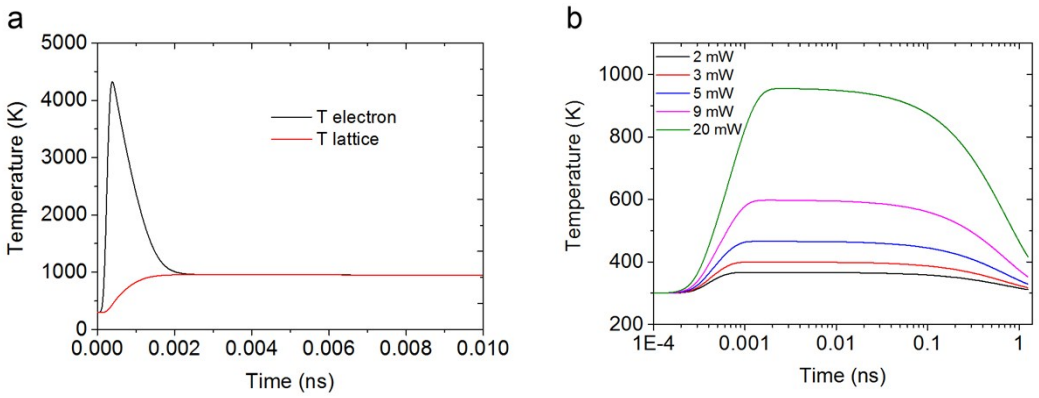

Supplementary Figure S2. (a) The calculated temperature variation of electrons (T_e) and lattice (T_l) of the Al nanostructure as a function of time after absorbing a 100 fs laser pulse (20 mW) using the TTM. (b) The calculated temperature sweep of Al nanorods excited by different laser powers: 2, 3, 5, 9 and 20 mW. The temperature evolution of Al nanostructures exhibits a transient sweep with a rapid raise in the first 1 to 2 picoseconds and a quick dissipation within 1 nanosecond.

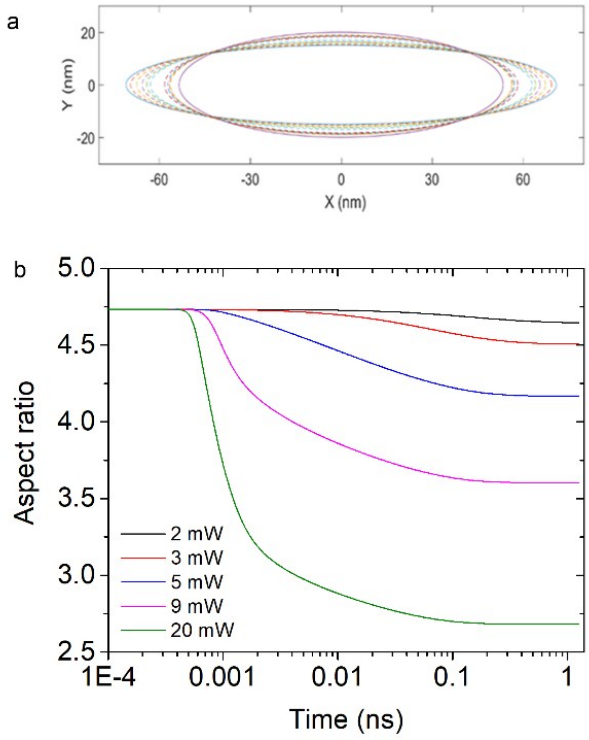

Supplementary Figure S3. (a) Surface diffusion driven shape transition trajectory of an Al nanorod with an initiation aspect ratio of ~4.7 by a 100 fs pulse (20 mW). Dashed circles indicate the shape profiles at various time frame (0.6, 0.7, 0.8, 0.9, 1, 2, 3, 4, 5 ps). (b) The aspect ratio evolution as a function of time for different laser powers.

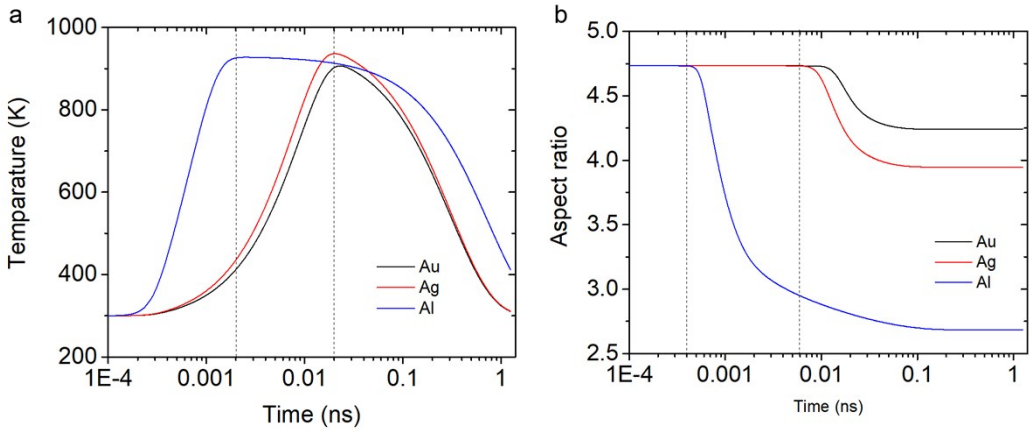

Supplementary Figure S4. Comparison of (a) lattice temperature and (b) aspect ratio evolutions for the nanorod made of three different materials: Au, Ag and Al, after absorbing the same amount of energy (85 pj). Clearly, the temperature of Al nanorod

rises to the peak value within 2 ps while that of Au and Ag both needs ~20 ps. The ultrafast heating leads to a faster shape transition for Al nanorods. The shape transition strength for Al nanorods is enormously pronounced than that of Au and Ag, implying lower energy consumption for reshaping Al nanorods. Indeed, our calculation shows that to achieve the same strength of shape transition, Al nanorods only need ~30% energy consumption of that for Au.

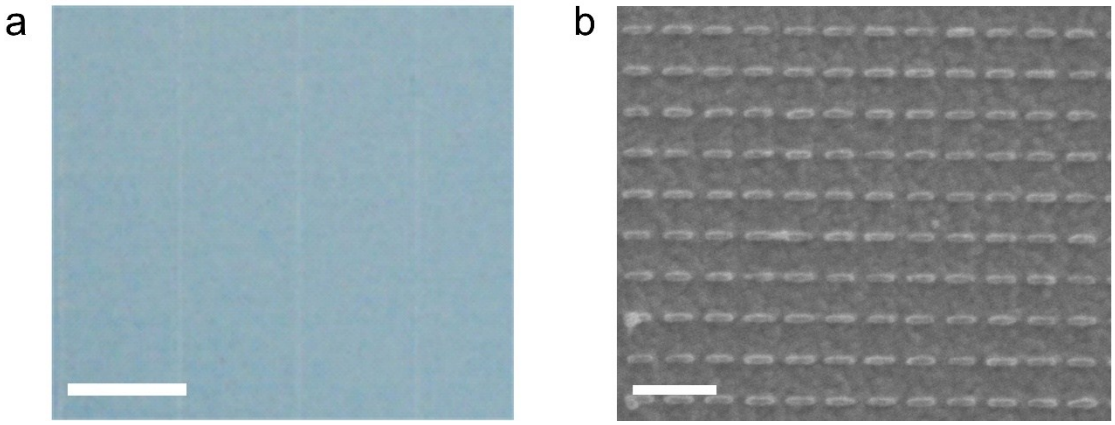

Supplementary Figure S5. (a) Optical microscope image of initial Al nanorod arrays. Scale bar: 20 μm. (b) The SEM image of Al nanorod arrays with an initial aspect ratio of ~4.7 before the laser processing. Scale bar: 400 nm.

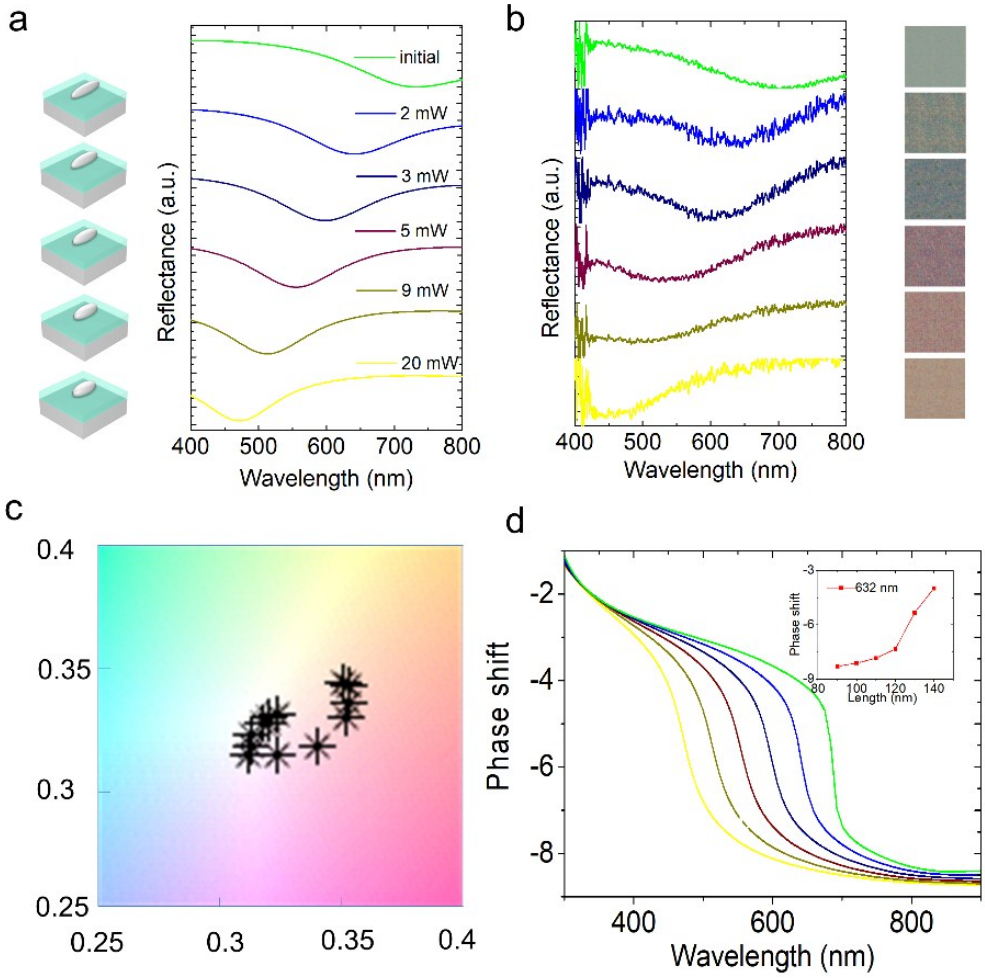

Supplementary Figure S6. Molding optical responses in color appearances and phase modulations. Numerical (a) and experimental (b) reflectance spectra of the initial nanorods (green) and reshaped ones at various laser powers (2, 3, 5, 9, 20 mW), respectively. (c) Chromaticity coordinates (CIE 1931 color space) of achieved reflection colors (black stars). (d) The simulated phase modulation as a function of the wavelength for reshaped Al nanorods by thermoplasmonic surface diffusion. The inset image shows the phase shift at the wavelength of 632 nm.

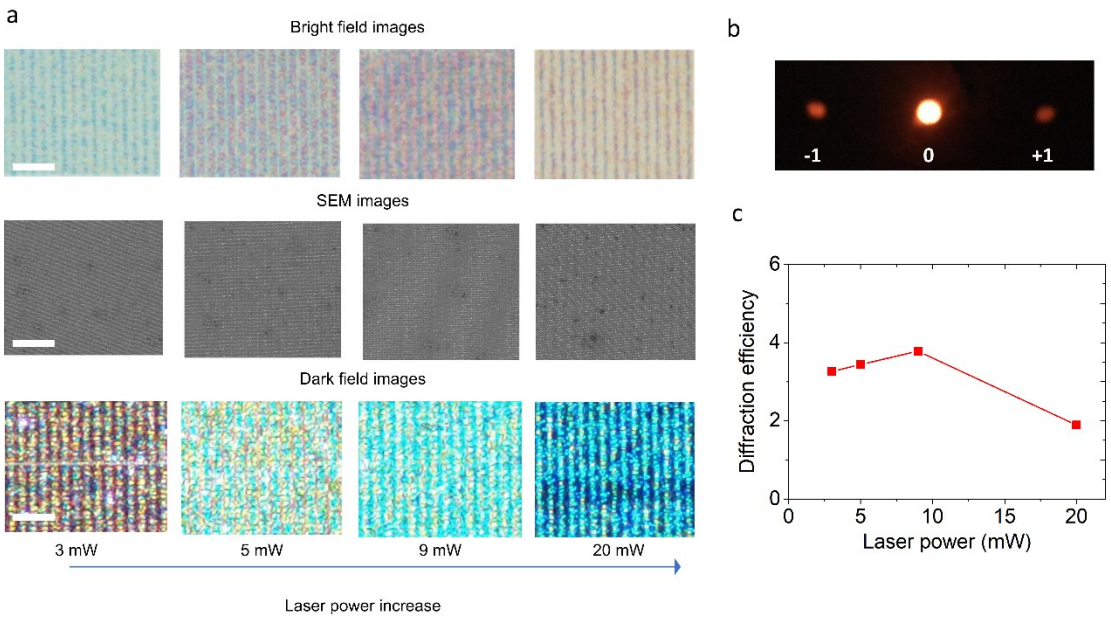

Supplementary Figure S7. (a) Bright field optical microscope images (first raw), SEM images (second raw) and dark field images (third raw) of grating structures by thermoplasmonic surface diffusion of Al nanorods at different powers (3, 5, 9, 20 mW). (b) A representative diffraction patterns by the fabricated gratings. (c) The measured diffraction efficiency at the wavelength of 632 nm for gratings achieved by variant laser powers.

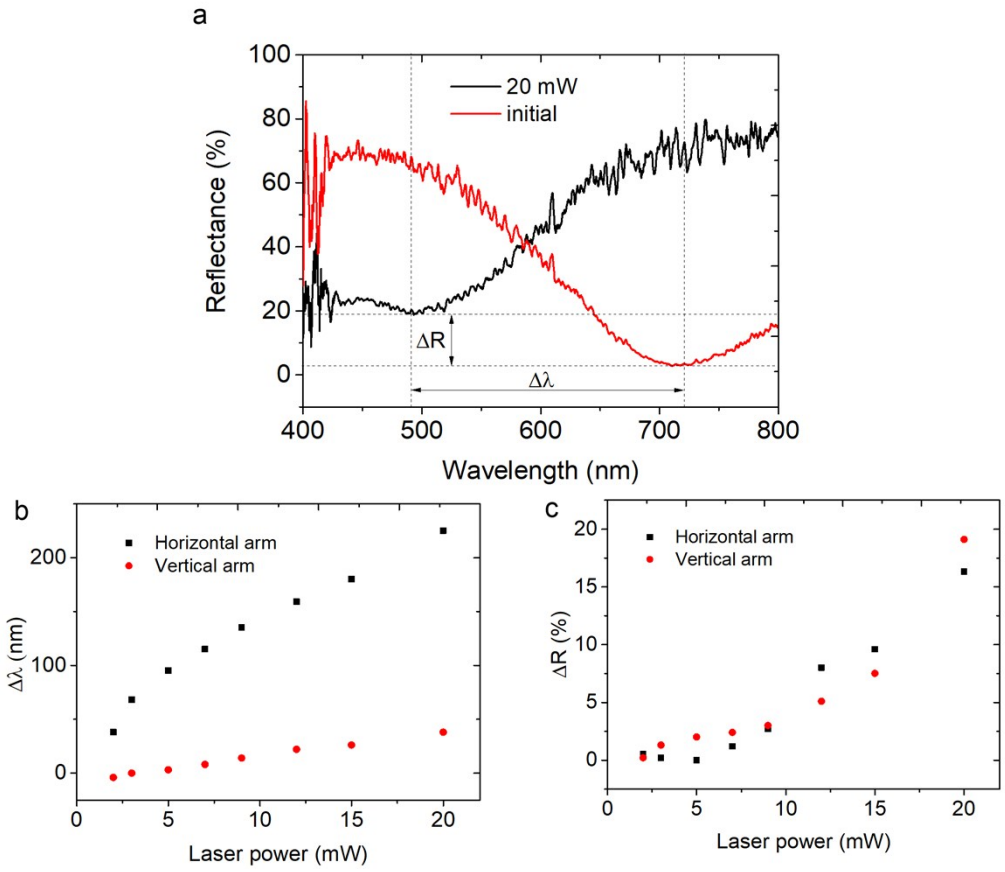

Supplementary Figure S8. (a) Illustration of the reflectance spectra before and after the surface diffusion driven shape transition of the horizontal arm of an Al cross structure. It reveals a distinct reflectance valley shift accompanied with an increase in the value of reflectance when the polarization is parallel to the horizontal arm. (b) The variation of the valley shifts of the reflectance spectra of the horizontal arm (black squares) and the vertical arm (red circles) as a function of laser powers. The horizontal arm by thermoplasmonic surface diffusion exhibits drastic shifts of the reflection valley over 200 nm whereas the vertical arm displays trivial shifts less than 30 nm. (c) The increase in reflectance of the horizontal arm (black squares) and the vertical arm (red circles) as a function of laser powers. Even the reflectance valley wavelength of the vertical arm keeps almost intact, an increased reflectance in the same level is observed compared with that of the horizontal arm.

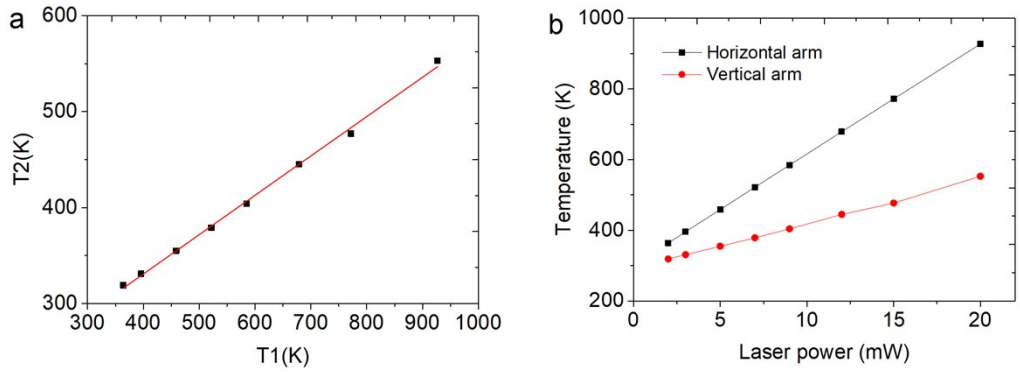

Supplementary Figure S9. (a) Simulated transient peak temperatures of the orthogonal arm (T2) as a function of the transient peak temperatures of the thermoplasmonic heated arm (T1). (b) Calculated transient peak temperatures of the two arms as a function of laser powers. The polarization of the incidence is parallel to the horizontal arm of the Al cross nanostructure. The calculation reveals that the vertical horizontal arm experiences much lower peak temperature compared with the thermoplasmonic heated vertical arm.

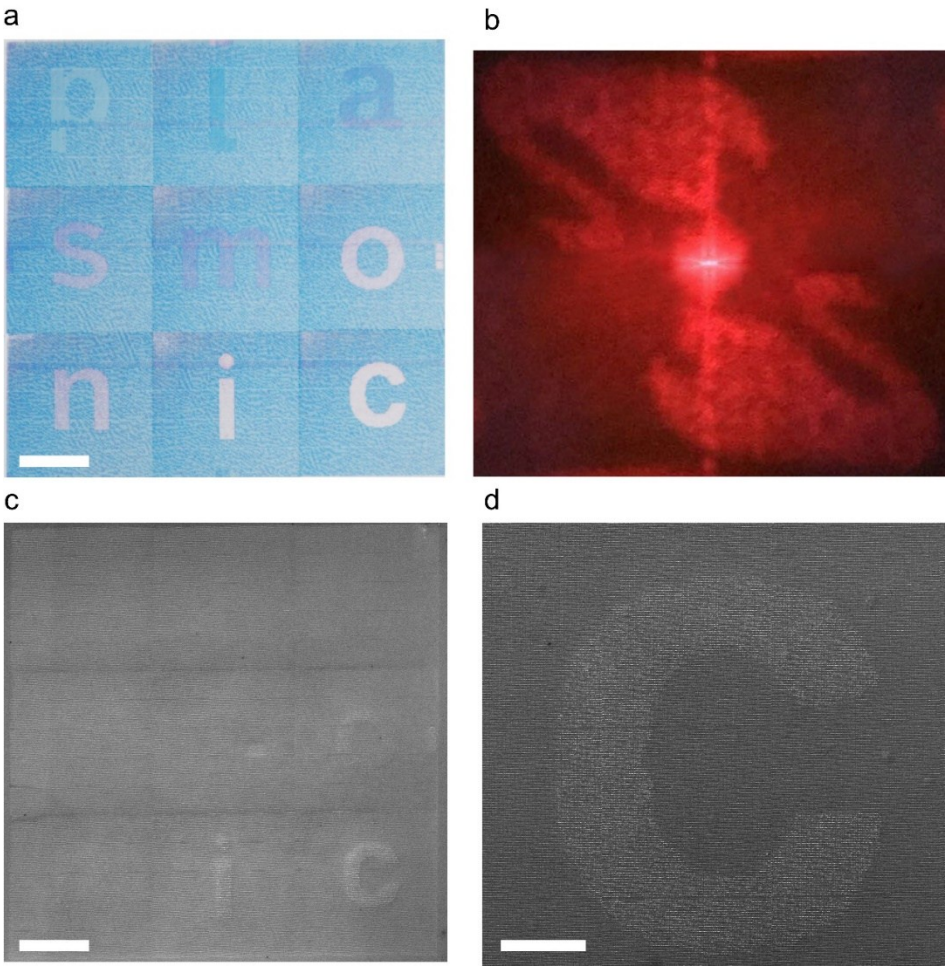

Supplementary Figure S10. Another collection of dual-function Janus metasurface. (a) The color image is retrieved from the reflection mode by horizontally-polarized white light illumination. Scale bar:50 μm. (b) Multiplexed holographic image is retrieved in the diffraction channel at the reconstruction wavelength of 632 nm with the vertical polarization. The SEM image (c) and zoom-in view (d) of the laser processed Al cross structures. Scale bar: 50 μm and 10 μm, respectively.

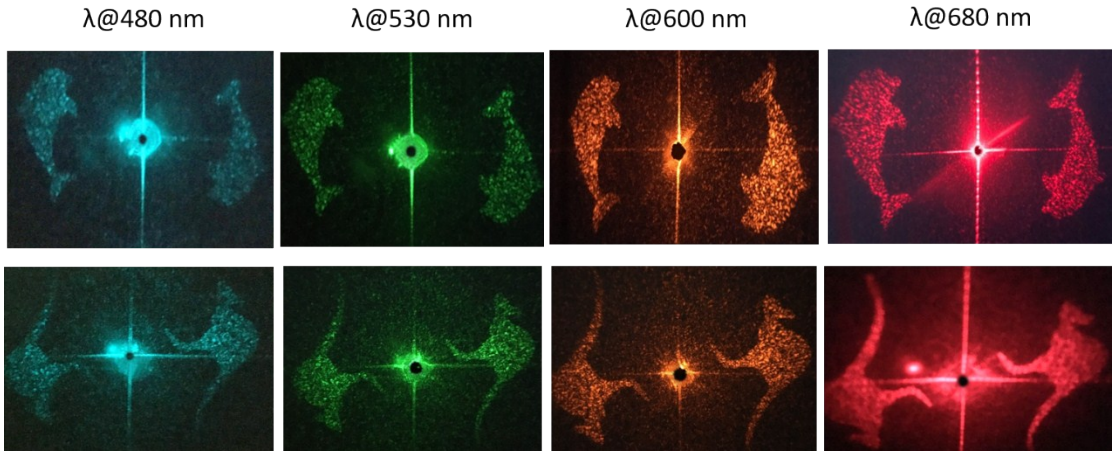

Supplementary Figure S11. Dual holograms encoded on orthogonal arms of the cross structures by laser printing. The holograms can operate at full visible frequencies over a bandwidth of ~200 nm, with an efficiency ~2%.

Reference

1. Guillaume, B.; Romain, Q., Thermo‐plasmonics: using metallic nanostructures as nano‐sources of heat. *Laser & Photonics Reviews* 2013, 7, 171-187.
2. Nichols, F. A.; Mullins, W. W., Morphological Changes of a Surface of Revolution due to Capillarity‐Induced Surface Diffusion. *J. Appl. Phys.* 1965, 36, 1826-1835.
3. Mullins, W. W., Mass transport at interfaces in single component systems. *Metallurgical and Materials Transactions A* 1995, 26, 1917-1929.
4. Taylor, A. B.; Siddiquee, A. M.; Chon, J. W. M., Below melting point photothermal reshaping of single gold nanorods driven by surface diffusion. *ACS Nano* 2014, 8, 12071-12079.
5. Inogamov, N. A.; Zhakhovskii, V. V.; Khokhlov, V. A., Jet formation in spallation of metal film from substrate under action of femtosecond laser pulse. *Journal of Experimental and Theoretical Physics* 2015, 120, 15-48.
6. Jiang, L.; Tsai, H. L., Improved two-temperature model and its application in ultrashort laser heating of metal films. *J. Heat Transfer* 2005, 127, 1167-1173.
7. Chen, J. K.; Tzou, D. Y.; Beraun, J. E., A semiclassical two-temperature model for ultrafast laser heating. *Int. J. Heat Mass Transfer* 2006, 49, 307-316.
8. Zhang, J.; Chen, Y.; Hu, M.; Chen, X., An improved three-dimensional two-temperature model for multi-pulse femtosecond laser ablation of aluminium. J. Appl. Phys. 2015, 117, 063104.